Program Digest, 2019 IEEE International Ultrasonics Symposium (IUS)
Glasgow, Scotland, October 6-9, 2019

Quantification of PSMA expression in prostate cancer by pharmacokinetic modeling of targeted ultrasound nanobubbles

Simona Turco
Department of Electrical Engineering
Eindhoven University of Technology
Eindhoven, the Netherlands
s.turco@tue.nl

Reshani H. Perera
Department of Radiology
Case Western Reserve University
Cleveland, OH, United States

Hessel Wijkstra
Departement of Urology
Amsterdam University Medical Center
Amsterdam, the Netherlands

Agata A. Exner
Department of Radiology
Case Western Reserve University
Cleveland, OH, United States

Massimo Mischi
Department of Electrical Engineering
Eindhoven University of Technology
Eindhoven, the Netherlands

***Abstract*—The value of contrast-enhanced ultrasound (CEUS) for prostate cancer diagnostics is still debated. Novel targeted ultrasound contrast agents enable visualization of molecular and cellular processes in vivo and non-invasively. Microbubbles targeted to the vascular endothelial growth factor receptor 2 have been successfully tested in humans, but detection rate for prostate cancer was limited to 65%. While microbubbles can only target molecules in the blood vessels, novel nanobubbles (NBs) can extravasate, thus enabling reaching targets beyond the vessel wall. Recently, NBs targeted to the prostate specific membrane antigen (PSMA), which is overexpressed by prostate cancer cells, have shown selective accumulation in prostate-tumor mouse models. However, methods for quantification of NB binding are still lacking. In this work, we propose a pharmacokinetic modeling approach to estimate the binding potential of PSMA-targeted NBs, and we test the proposed method in 7 dual-tumor mouse models of prostate cancer.**

***Index Terms*—ultrasound contrast agents, prostate cancer, molecular imaging, pharmacokinetic modelling, nanobubbles**

I. Introduction

With more than 1 million new cases and about 360,000 deaths each year, prostate cancer is the most common form of cancer and the second cause of cancer-related deaths among men worldwide [1]. Prostate cancer diagnosis still relies on repeated systematic biopsies, often triggered by an elevated serum prostate-specific antigen (PSA) [2]. Besides the high risk of infection, often leading to hospitalization, biopsies result in both over-diagnosis and under-treatment [3]–[5]. Moreover, they cannot provide accurate tumor localization, hampering the use of available focal therapies. As a result, the recommended treated options for localized disease are still radiotherapy and radical prostatectomy, with associated severe side effects, co-morbidities, and reduced quality of life [5]. This highlights the urgent need for reliable imaging methods providing accurate prostate cancer detection and localization.

Contrast-enhanced ultrasound (CEUS) has received increasing attention for imaging of prostate cancer. By intravenous injection of echo-enhancing microbubbles, which act as intravascular reflectors, combined with contrast-specific ultrasound scanning sequences, CEUS permits non-invasive vascular assessment down to the microcirculation [6]. Of special interest is neo-vascularization in cancer, a process known as angiogenesis [7]. Promoted by the over-expression of pro-angiogenic factors, tumor angiogenesis results in a chaotic network of leaky microvessels, exhibiting higher density, tortuousity and arterio-venous shunts [7]. Analysis of time-intensity curves (TICs) extracted from CEUS loops by indicator dilution theory permits estimation of (semi)quantitative parameters, related to perfusion and contrast dispersion, which have shown to reflect abnormalities in tumor vasculature [8], [9]. However, despite reported improvements, visual inspection and (semi)quantitative analysis of CEUS are not sufficiently accurate to replace biopsies [6], [10].

Molecular imaging of prostate cancer has recently become possible thanks to the introduction of microbubbles targeted to the vascular endothelial growth receptor receptor 2 (VEGFR2), an established pro-angiogenic factor over-expressed in several solid tumors [11], [12]. Despite showing promise, however, the detection rate for prostate cancer in a phase-0 clinical trial was still limited to 65% [11].

More effective contrast agents are needed to improve diagnostic accuracy. Novel nanobubbles (NBs) are opening new avenues for molecular ultrasound imaging. With a diameter about ten times smaller than microbubbles (~0.3 μm vs 1-10 μm), NBs can cross the vascular endothelium, especially in case of enhanced permeability, such as in tumor vasculature [13], [14]. Besides permitting for the first time the assessment of extravascular leakage by ultrasound imaging, NBs also enable a whole new spectrum of possibilities for targeting

978-1-7281-4595-2/19/$31.00 ©2019 IEEE

beyond the vessel wall.

In this context, a NB targeted to the prostate-specific membrane antigen (PSMA), which is typically over-expressed on the cell membrane of prostate cancer cells, has been developed and tested [15]. Although prolonged retention was observed in-vivo, and selective accumulation was confirmed by ex-vivo histological analysis, methods for in-vivo quantification of extravasation and binding are currently lacking. Compared to microbubbles, in fact, targeted NBs exhibit more complex kinetics, involving transport in the circulation, extravasation in tissue and binding on cell membrane. As a result, established quantification methods used for CEUS are not suitable.

In this work, we propose a pharmacokinetic modeling framework to describe targeted-NBs transport and assess extravasation and binding in-vivo. Based on the similar kinetics, the simplified reference tissue model, originally developed for receptor kinetics studies in the context of nuclear imaging, is here adapted for quantification of targeted NBs by CEUS. The proposed framework is validated in 7 dual-tumor mouse models of prostate cancer.

II. Methods

A. Pharmacokinetic modeling

PSMA-targeted NBs travel troughtout the circulation, may cross the vascular wall, and may attach on the membrane of cells overexpressing PSMA. The kinetics of PSMA-targeted NBs can thus be desrcibed by a pharmacokinetic model with three compartments: the plasma compartment, the free tissue compartment, where no specific NB binding occurs, and the bound tissue compartment, where specific NB binding may occur. If a reference tissue is available, i.e., a tissue without specific binding, the kinetics of targeted-NB are described by the following differential equations

$$\frac{dC_r(t)}{dt} = K_1' C_p(t) - k_2' C_r(t), \tag{1}$$

$$\frac{dC_f(t)}{dt} = K_1 C_p(t) - k_2 C_r(t) - k_3 C_f(t) + k_4 C_b(t), \tag{2}$$

$$\frac{dC_b(t)}{dt} = K_3 C_f(t) - k_4 C_b(t), \tag{3}$$

where $C_p(t), C_f(t), C_b(t)$, and $C_r(t)$ are the concentrations of NBs in the plasma, free, bound, and reference tissue compartments, respectively; K_1 (ml·ml $^{-1}\cdot$ min^{-1}) is the rate constant for transfer from plasma to free compartment; k_2 is the rate constant for transfer from free to plasma compartment (min^{-1}); k_3 is the rate constant for transfer from free to bound compartment (min^{-1}); k_4 is the rate constant for transfer from bound to free compartment; K_1' is the rate constant for transfer from plasma to reference compartment (ml·ml^{-1}·min^{-1}); k_2' is the rate constant for transfer from reference to plasma compartment (min^{-1}).

In case the kinetics of the free and bound compartment are difficult to distinguish, the differential equations are simplified by substituting (2) and (3) by

$$\frac{dC_t(t)}{dt} = K_1 C_p(t) - k_{2a} C_t(t), \tag{4}$$

where $C_t(t)$ is the NB concentration in the target tissue, and k_{2a} (min^{-1}) is the apparent (overall) rate constant for transfer from target compartment to plasma, for which the following relationship should hold

$$\frac{K_1}{k_{2a}} = \frac{K_1}{k_2}(1 + \mathrm{BP}), \tag{5}$$

with BP being the binding potential defined as BP= k_3/k_4. Although in practice the concentrations $C_t(t)$ and $C_r(t)$ are not available, a linear relationship between the acoustic intensity and the contrast concentration can be assumed, provided that time-intensity curves (TICs) obtained from CEUS loops are properly linearized. Then, defining the ratio $R1 = K_1/K_1'$, the solution of the simplified reference tissue model for CEUS imaging can be obtained as

$$I_t(t) = R_1 I_r(t) + \left(k_2 - \frac{R_1 k_2}{1+\mathrm{BP}}\right) I_r(t) * e^{-\frac{k_2}{1+\mathrm{BP}}t}, \tag{6}$$

where $I_t(t) = G{\cdot}C_t(t)$ and $I_r(t) = G{\cdot}Cr(t)$ are the linearized acoustic intensity over time in the target and reference tissues, respectively, and G is a multiplicative constant.

B. Dual-tumor mouse model

Four to six weeks old male athymic nude mice were anesthetized with inhalation of 3% isoflurane with 1L/min oxygen. A dual-tumor model was obtained in each mouse by subcutaneous injection of PSMA-positive PC3pip cells in one flank, and PSMA-negative PC3flu cells in the other flank, as described in [15]. Mice were kept under observation until tumors reached ~0.8 cm in diameter. Animal experiments were conducted according to a protocol approved by the Institutional Animal Care and Use Committee (IACUC) at Case Western Reserve University.

C. Ultrasound imaging

CEUS was performed by injection of a 200-μL bolus of either non-targeted NBs or PSMA-targeted NBs, which were prepared according to [15]. A Toshiba Scanner (AplioXG SSA-790A, Toshiba Medical Imaging Systems, Otawara-Shi, Japan) was used with a PLT-1204BT probe working at 12 MHz (MI, 0.1; dynamic range, 65dB; gain, 70dB; imaging frame rate, 0.2 frames/s). The probe was placed so as to visualize both tumors in the same field of view. After about 30 min, repeated high-intensity flashes were applied to destroy any residual NB. The other agent (non-targeted NBs or PSMA-targeted NBs) was administered with the same protocol, after a waiting period of 30 min. Regions of interest (ROIs) were drawn on both PSMA-positive and PSMA-negative tumors, and TICs for each ROI were extracted and linearized for further processing. Two mice were excluded from analysis after visual inspection of TICs, which revealed large artefacts including peak saturation, amplitude distortion, and delayed start of recording.

D. Parameter estimation

For both NB types, the linearized TICs from the PSMA-positive tumor were fit by the model in (6) to estimate the binding potential, BP. The TICs obtained from the PSMA-negative tumor were used as reference tissue, i.e., $I_r(t)$ in (6). Prior to fitting, both TICs were interpolated and oversampled by a factor 3 and filtered by a Savitzy-Golay filter. Furthermore, the reference TIC was fit by an analytical function (model 1) proposed by Orton et al. [16] in the context of pharmacokinetic modeling for dynamic contrast-enhanced MRI.

A basis function method was used to increase robustness and decrease computation time of parameter estimation [17]. Defining $\theta_1 = R_1$, $\theta_2 = k_2 - \frac{R_1 k_2}{1+\mathrm{BP}}$ and $\theta_3 = \frac{k_2}{1+\mathrm{BP}}$ and rewriting (6) as

$$I_t(t) = \theta_1 I_r(t) + \theta_2 I_r(t) * e^{-\theta_3 t}, \tag{7}$$

an equation linear in the parameters θ_1 and θ_2 is obtained. The remaining non-linear term is addressed by defining the following set of basis functions

$$B_i(t) = I_r(t) * e^{-\theta_{3i} t}. \tag{8}$$

By setting suitable parameter bounds for θ_3, a fine grid of B_i can be generated by calculating all the convolutions in (8) prior to linear regression of (6), considerably speeding up the estimation algorithm. Limiting k_2 between 10^{-7} min^{-1} and 10 min^{-1}, and BP between 0 and 10, resulted in a range for θ_3 between 10^{-8} min^{-1} and 5 min^{-1}, which was spanned for 5000 equally-spaced samples.

III. Results

The estimated parameters obtained for the mice included in the analysis are reported in Table I. The estimated BP values were larger for PSMA-targetd NBs in three mice, smaller for PSMA-targetd NBs in one mouse, and equal to zero for both NB types in one mouse. Figure 1 shows examples of TICs obtained in the reference tissue ($I_r(t)$, grey circles) and target tissue ($I_t(t)$, black stars), together with the corresponding fit (solid black line). In line with the estimated BP equal to zero, a return to baseline in the late phase is observed for both NB types for 'mouse3' (Fig. 1(a,b)), while the longer retention observed for the PSMA-targeted NBs (Fig. 1(b)) is reflected by a larger k_2, which represents the transfer constant from plasma to the free tissue compartment. Conversely, in 'mouse5', a steady plateau is observed in the late phase for PSMA-targeted NBs (Fig. 1(d)), which is in line with the estimated high BP (Table I).

TABLE I
Estimated parameter values for non-targeted NBs and PSMA-targeted NBs for all mice.

	Non-targeted NBs		**PSMA-targeted NBs**	
	k_2 (min^{-1})	BP (-)	k_2 (min^{-1})	BP (-)
mouse1	0.04	0.83	0.31	0.28
mouse2	4.20	0.29	0.06	0.42
mouse3	1.21	0.00	1.85	0.00
mouse4	1.40	0.03	0.26	0.18
mouse5	5.04	0.63	0.04	10.00

IV. Discussion and conclusions

In this work, the reference tissue model was proposed to describe the extravasation and binding kinetics of PSMA-targeted NBs. Fitting linearized TICs extracted form CEUS by the proposed model enables asssessment of vascular permeability and PSMA expression by the estimation of the transfer rate constant, k_2, and the binding potential, BP.

The estimated BP was larger for PSMA-targeted NBs compared to non-targeted NBs in most of the mice included in the analysis. This is in line with previous finding reporting prolonged retention and selective accumulation of PSMA-targeted NBs, and confirms the potential of these novel agents for quantification of PSMA expression in prostate cancer [15].

Although non-zero BP values were obtained for non-targeted NBs, it should be noted that BP =k_3/k_4, and thus reflects both binding (k_3) and unbinding (k_4), suggesting that non-specific binding may still occur for non-targeted NBs. In fact, histological analysis has shown that both targeted and untargeted NBs are seen in extracted tumor tissue, with the targeted NBs showing a higher degree of retention after 30 min [15]. The smaller BP obtained in one mouse for PSMA-targeted NBs compared to non-targeted NBs could be due to higher non-specific binding of targeted NBs compared to actual binding of PSMA-targeted NBs in this tumor. Another possible explanation could be inaccuracy in the estimation of k_2 and BP. In the future, sensitivity analysis will be performed to analyze possible correlation between parameters and clarify whether some parameters are weakly identifiable.

An estimated BP equal to zero for both PSMA-targeted and non-targeted NBs was observed in one mouse. Accordingly, a complete contrast wash-out was observed in the late phase (Fig. 1(a,b)). This might be due to several causes, including heterogeneous vascularity and vascular permeability of this tumor, low NB targeting efficiency, or low PSMA expression in the PSMA-positive tumor. Although immunochemistry analysis in comparable dual-tumor mouse models has previously confirmed higher PSMA expression in PSMA-postive tumors [15], immuno-histological quantification of ex-vivo tumors was not performed in this study. This is necessary to provide accurate validation of the proposed BP parameter for in-vivo assessment of PSMA expression and it will be pursued in future studies.

Finally, a limitation of the proposed reference tissue model is the need for a reference tissue in the field of view. In the future, alternative pharmacokinetic models could be investigated that include modeling of the contrast plasma concentration, similar to [12], permitting additional assessment of the vascular compartment, and avoiding the need to measure the concentration in the reference tissue.

To conclude, pharmacokinetic analysis of the kinetics of PSMA-targeted NBs by the simplified reference tissue model is feasible. Although the binding potential, BP, represents a promising parameter for quantitative assessment of PSMA expression in prostate tumors, further validation against ex-

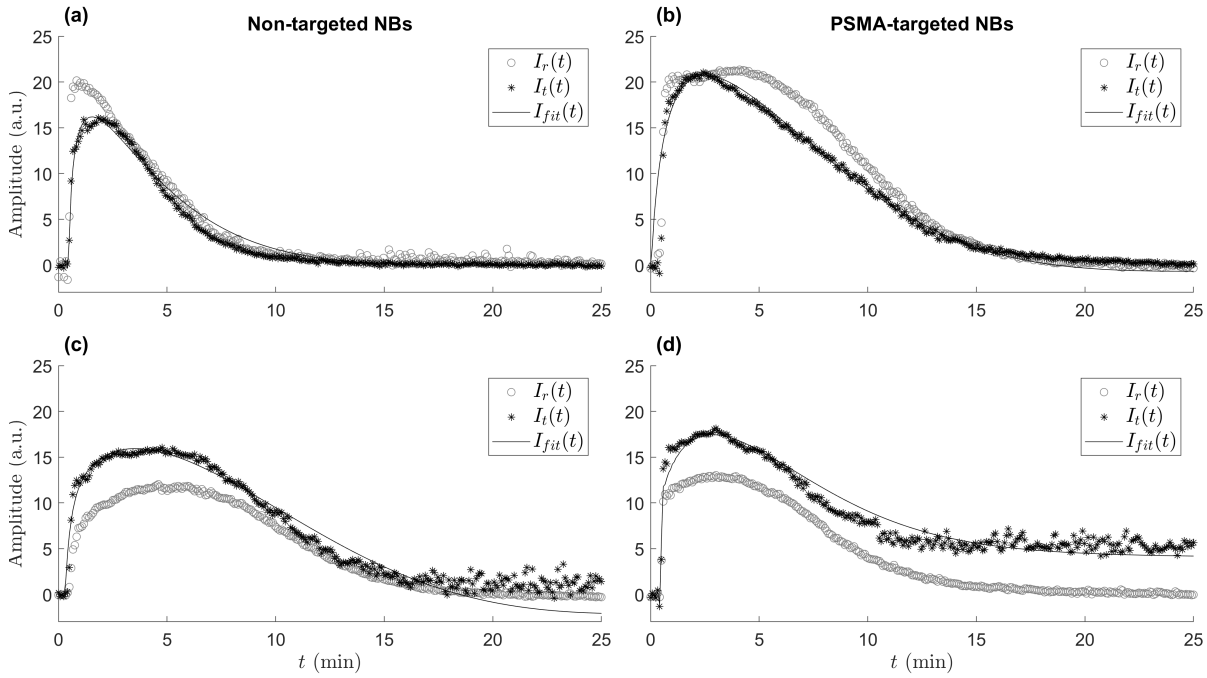

Fig. 1. Examples of TICs obtained in the reference ($I_r(t)$, grey circles) and target tissue ($I_t(t)$, black stars), together with corresponding model fit (solid black line) obtained in 'mouse3' (a,b) and 'mouse5' (c,d) for non-targeted NBs (a,c) and PSMA-targeted NBs (b,d).

vivo immuno-histological analysis is necessary to confirm the promising results.

REFERENCES

[1] F. Bray, J. Ferlay, I. Soerjomataram, R. L. Siegel, L. A. Torre, and A. Jemal, "Global cancer statistics 2018: Globocan estimates of incidence and mortality worldwide for 36 cancers in 185 countries," *CA: a cancer journal for clinicians*, vol. 68, no. 6, pp. 394–424, 2018.

[2] A. Heidenreich, P. J. Bastian, J. Bellmunt, M. Bolla, S. Joniau, T. van der Kwast, M. Mason, V. Matveev *et al.*, "Eau guidelines on prostate cancer. part 1: screening, diagnosis, and local treatment with curative intentupdate 2013," *European urology*, vol. 65, no. 1, pp. 124–137, 2014.

[3] E. C. Serefoglu, S. Altinova, N. S. Ugras, E. Akincioglu, E. Asil, and M. D. Balbay, "How reliable is 12-core prostate biopsy procedure in the detection of prostate cancer?" *Canadian Urological Association Journal*, vol. 7, no. 5-6, p. E293, 2013.

[4] R. Kvåle, B. Møller, R. Wahlqvist, S. D. Fosså, A. Berner, C. Busch, A. E. Kyrdalen, A. Svindland *et al.*, "Concordance between gleason scores of needle biopsies and radical prostatectomy specimens: a population-based study," *BJU international*, vol. 103, no. 12, pp. 1647–1654, 2009.

[5] N. Mottet, J. Bellmunt, M. Bolla, E. Briers, M. G. Cumberbatch, M. De Santis, N. Fossati, T. Gross *et al.*, "Eau-estro-siog guidelines on prostate cancer. part 1: screening, diagnosis, and local treatment with curative intent," *European urology*, vol. 71, no. 4, pp. 618–629, 2017.

[6] A. Maxeiner, T. Fischer, J. Schwabe, A. D. J. Baur, C. Stephan, R. Peters, T. Slowinski, M. von Laffert *et al.*, "Contrast-enhanced ultrasound (ceus) and quantitative perfusion analysis in patients with suspicion for prostate cancer," *Ultraschall in der Medizin-European Journal of Ultrasound*, vol. 40, no. 03, pp. 340–348, 2019.

[7] J. Folkman, "Angiogenesis in cancer, vascular, rheumatoid and other disease," *Nature medicine*, vol. 1, no. 1, p. 27, 1995.

[8] M. Mischi, S. Turco, O. I. Soliman, J. Folkert, H. Wijkstra, and I. Schoots, *Quantification of contrast kinetics in clinical imaging*. Springer, 2018.

[9] S. Turco, H. Wijkstra, and M. Mischi, "Mathematical models of contrast transport kinetics for cancer diagnostic imaging: a review," *IEEE reviews in biomedical engineering*, vol. 9, pp. 121–147, 2016.

[10] Y. Li, J. Tang, X. Fei, and Y. Gao, "Diagnostic performance of contrast enhanced ultrasound in patients with prostate cancer: a meta-analysis," *Academic radiology*, vol. 20, no. 2, pp. 156–164, 2013.

[11] M. Smeenge, F. Tranquart, C. K. Mannaerts, T. M. de Reijke, M. J. van de Vijver, M. P. Laguna, S. Pochon, J. J. de la Rosette *et al.*, "First-in-human ultrasound molecular imaging with a vegfr2-specific ultrasound molecular contrast agent (BR55) in prostate cancer: a safety and feasibility pilot study," *Investigative radiology*, vol. 52, no. 7, pp. 419–427, 2017.

[12] S. Turco, I. Tardy, P. Frinking, H. Wijkstra, and M. Mischi, "Quantitative ultrasound molecular imaging by modeling the binding kinetics of targeted contrast agent," *Physics in Medicine & Biology*, vol. 62, no. 6, p. 2449, 2017.

[13] A. de Leon, R. Perera, C. Hernandez, M. Cooley, O. Jung, S. Jeganathan, E. Abenojar, G. Fishbein *et al.*, "Contrast enhanced ultrasound imaging by nature-inspired ultrastable echogenic nanobubbles." *Nanoscale*, vol. 11, no. 33, p. 15647, 2019.

[14] R. H. Perera, C. Hernandez, H. Zhou, P. Kota, A. Burke, and A. A. Exner, "Ultrasound imaging beyond the vasculature with new generation contrast agents," *Wiley Interdisciplinary Reviews: Nanomedicine and Nanobiotechnology*, vol. 7, no. 4, pp. 593–608, 2015.

[15] R. Perera, X. Wang, Y. Wang, G. Ramamurthy, P. Peiris, E. Abenojar, J. P. Basilion, A. A. Exner *et al.*, "Real time ultrasound molecular imaging of prostate cancer with psma-targeted nanobubbles," *bioRxiv*, p. 634444, 2019.

[16] M. R. Orton, J. A. d'Arcy, S. Walker-Samuel, D. J. Hawkes, D. Atkinson, D. J. Collins, and M. O. Leach, "Computationally efficient vascular input function models for quantitative kinetic modelling using dce-mri," *Physics in Medicine & Biology*, vol. 53, no. 5, p. 1225, 2008.

[17] R. N. Gunn, A. A. Lammertsma, and V. J. Cunningham, "Parametric imaging of ligand-receptor interactions using a reference tissue model and cluster analysis," in *Quantitative functional brain imaging with positron emission tomography*. Elsevier, 1998, pp. 401–406.